

# Guided Diffusion from Self-Supervised Diffusion Features

Vincent Tao Hu<sup>1,2\*</sup>, Yunlu Chen<sup>3</sup>, Mathilde Caron<sup>4</sup>,  
Yuki M. Asano<sup>2</sup>, Cees G. M. Snoek<sup>2</sup>, Björn Ommer<sup>1</sup>

<sup>1</sup>CompVis Group, LMU Munich, <sup>2</sup>University of Amsterdam, <sup>3</sup>CMU, <sup>4</sup>Google Research

## Abstract

Guidance serves as a key concept in diffusion models, yet its effectiveness is often limited by the need for extra data annotation or classifier pretraining. That is why guidance was harnessed from self-supervised learning backbones, like DINO. However, recent studies have revealed that the feature representation derived from diffusion model itself is discriminative for numerous downstream tasks as well, which prompts us to propose a framework to extract guidance from, and specifically for, diffusion models. Our research has yielded several significant contributions. Firstly, the guidance signals from diffusion models are on par with those from class-conditioned diffusion models. Secondly, feature regularization, when based on the Sinkhorn-Knopp algorithm, can further enhance feature discriminability in comparison to unconditional diffusion models. Thirdly, we have constructed an online training approach that can concurrently derive guidance from diffusion models for diffusion models. Lastly, we have extended the application of diffusion models along the constant velocity path of ODE to achieve a more favorable balance between sampling steps and fidelity. The performance of our methods has been outstanding, outperforming related baseline comparisons in large-resolution datasets, such as ImageNet256, ImageNet256-100 and LSUN-Churches. Our code will be released.

## 1. Introduction

Diffusion models have shown significant advancements in computer vision, including image processing [42], video analysis [20], point cloud processing [52], and human pose estimation [15]. Typically, these applications rely on guidance signals to enhance controllability based on user preferences, resulting in improved fidelity [13, 43]. However, these applications often heavily depend on labor-intensive annotations, such as image-text pairs [41] or image-label pairs [12]. Annotating the data is time-consuming, error-prone and may inject bias. In our work, we aim to address this guidance requirement by eliminating the need for data

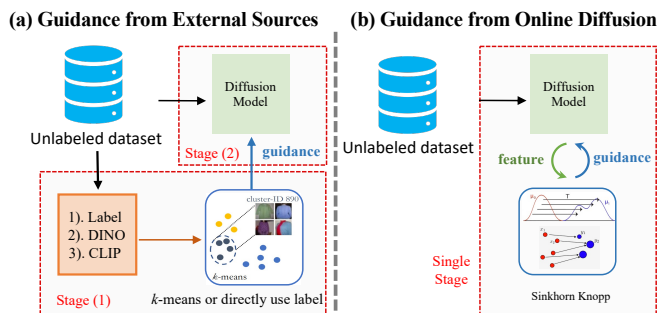


Figure 1. Previous works derive the external guidance signal from burdensome label annotation, or self-supervised representations to improve fidelity in a complex two-stage manner. Our work, however, boosts performance by using the diffusion model itself to achieve online self-guidance in a single stage.

annotations.

A few studies [4, 16, 22] have explored the possibility of harnessing self-supervised representations to provide annotation-free training for diffusion models. Concurrently, the features extracted by diffusion models themselves have found utility across diverse representation learning [55] and image correspondence tasks [34, 50], which illustrates the significant potential for leveraging diffusion models in discriminative tasks. On the other hand, diffusion models have evolved into a more versatile form, encompassing both the Stochastic Differential Equation (SDE) approach, such as Variance-Preserving SDE [19] and Variance-Exploding SDE [47], as well as the Ordinary Differential Equation (ODE) approach [1, 29, 31]. Notably, ODE-based models tend to strike a more favorable balance between sampling efficiency and quality compared to SDE-based counterparts, as demonstrated in [26]. Given that self-guidance and generalized diffusion models offer two crucial components for advancing generative learning, the natural progression is to explore the integration of self-guidance within the framework of generalized diffusion models.

In this work, we introduce a novel framework that harnesses the inherent guidance capabilities of the diffusion model itself, as illustrated in Figure 1. Our contributions encompass three key aspects: Firstly, we demonstrate the

\*Part of this work was done while at University of Amsterdam.

feasibility of directly extracting guidance signals from diffusion models themselves, eliminating the reliance on self-supervised learned backbones (e.g., DINO [8]). Secondly, we introduce an online optimal-transport-based algorithm to extract guidance signals from diffusion models, yielding substantial performance improvements for these models. Our approach outperforms unconditional generation by leveraging the same amount of *unlabelled* data and achieves results that are comparable to both clustering-based guidance signals and class-conditioned guidance. Finally, our method not only generates images based on user query inputs but also successfully achieves an effective equilibrium between sampling speed and fidelity.

## 2. Related works

**Exploiting features in diffusion models.** Diffusion Models [19, 46, 48] have demonstrated their versatility across various domains [42, 43]. Recently, it has been shown that diffusion models can be beneficial for discriminative tasks such as classification [35], semi-supervised learning [56], and more specific downstream tasks like human pose estimation [15, 21, 40] and representation learning [55]. From another perspective, the intermediate features of these models have been exploited in various computer vision applications, such as image correspondence [34, 50], even cross-modality correspondences [51], scene geometry, support relations, shadows and depth [58], open-vocabulary object segmentation [28, 54], and few-shot segmentation [30]. In this paper, we take a step further to explore the possibility of utilizing features from diffusion models to further bootstrap its self-guidance.

**Guidance in diffusion models.** Diffusion models excel in controllable generative modeling, owing to their capacity of guidance for enhanced controllability [42] and fidelity [13]. To leverage the performance of pretrained diffusion models and utilize the mathematical principles underlying the score in diffusion models, Dhariwal and Nichol [13] suggest training an additional classifier on noisy data to guide unconditional diffusion models. Complementing this, Ho *et al.* [18] propose classifier-free guidance, which involves random dropout of the guidance signal to integrate the capabilities of both unconditional and conditional sampling within a singular network. Nevertheless, these approaches still require data annotation during training.

Recent efforts [4, 22] aim to eliminate the need for data annotation, capitalizing on advancements in self-supervised learning [3, 7, 8]. They utilize external self-supervised learned backbones to extract guidance signals for image, box, and pixel-level guidance, achieving high-fidelity generation without relying on data annotation. Several existing works such as Slot-diffusion [24, 53] also address this problem through the lens of object-centric learning, often requir-

ing extra self-supervised learning encoders, particularly in complex scenarios. Unlike all of them, our work eliminates the reliance on external self-supervised models. Instead, we exploit guidance from the diffusion model itself. This is achieved through an optimal-transport assignment during training, enabling the model to cultivate its own guidance mechanism.

## 3. Preliminaries

We design our online guidance based on the generalized diffusion framework, chosen for its flexibility, simplicity, and efficient sampling capabilities. We will illustrate its basics through both stochastic and deterministic perspectives.

**Stochastic diffusion probabilistic models.** Given samples from an underlying data distribution  $\mathbf{x}_0 \sim p_0$ , the goal of a diffusion probabilistic model [19, 47] is to fit the distribution and enable the generation of novel examples through sampling. The diffusion process gradually corrupts the sample  $\mathbf{x}_0$  with noise to  $\mathbf{x}_t$  in a continuous time schedule  $t \in [0, T]$  until  $p_T(\mathbf{x}_T)$  becomes random noise, described as a stochastic differential equation (SDE) [48]:

$$d\mathbf{x} = \mathbf{f}(\mathbf{x}, t) dt + g(t) d\mathbf{w}, \quad (1)$$

where  $\mathbf{w}$  is the standard Wiener process,  $\mathbf{f}(\mathbf{x}, t)$  is the vector-valued drift coefficient,  $g(t)$  is the scalar diffusion coefficient. The reverse-time SDE diffusion process generates data starting by sampling from  $p_T(\mathbf{x}_T)$  [2, 48]:

$$d\mathbf{x} = [\mathbf{f}(\mathbf{x}, t) - g^2 \nabla_{\mathbf{x}} \log p_t(\mathbf{x})] dt + g(t) d\bar{\mathbf{w}}, \quad (2)$$

where  $\nabla_{\mathbf{x}} \log p_t(\mathbf{x})$  is known as the score function of the noise-perturbed data distribution,  $\bar{\mathbf{w}}$  is a reverse-time standard Wiener process,.

**Deterministic diffusion models.** For any diffusion process, there exists a corresponding deterministic process with the same marginal probability densities in the form of an ODE. As an example, Song *et al.* [48] introduce a deterministic Probability flow ODE, where the velocity in probabilistic flow ODE has the form

$$v_t(\mathbf{x}_t, t) = \mathbf{f}(\mathbf{x}_t, t) - \frac{g_t^2}{2} \nabla \log p_t, \quad (3)$$

where  $d\mathbf{x} = v_t(\mathbf{x}_t, t) dt$ . It is shown in [26, 27] that using ODE sampler of the form Equation 3 can reduce sampling costs compared to sampling with discretization of the diffusion SDE in Equation 2.

When provided with empirical observations of the data distribution  $\mathbf{x}_0 \sim p_0$  and typically Gaussian noise distribution  $\mathbf{x}_1 \sim p_1$ , the objective within the deterministic Ordinary Differential Equation (ODE) framework is to estimate

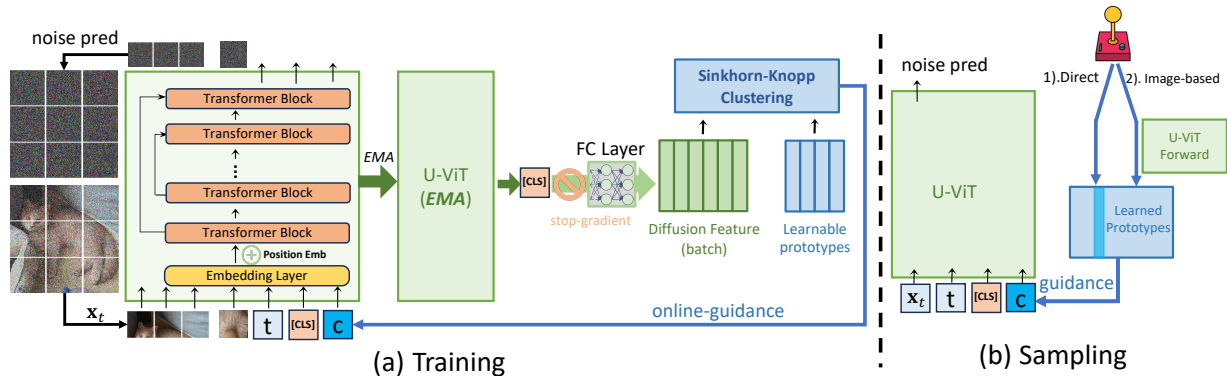


Figure 2. **Our Framework.** Our method leverages the inherent guidance capabilities of diffusion models during training by incorporating the optimal-transport loss. In the sampling phase, we can condition the generation on either the learned prototype or by an exemplar image.

a coupling function  $\pi(p_0, p_1)$  that characterizes the transition between these two distributions. This objective could be formulated as solving an ODE:

$$d\mathbf{x}_t = v(\mathbf{x}_t, t)dt, \quad (4)$$

over time  $t \in [0, 1]$ , where the velocity  $v : \mathbb{R}^d \times [0, 1] \rightarrow \mathbb{R}^d$  is set to drive the flow from  $p_0$  to  $p_1$ .

Usually, the drift (velocity)  $v_\theta(\mathbf{x}_t, t)$  can be represented by a neural network, and the loss can be formulated in a regression manner:

$$\hat{\theta} = \arg \min_{\theta} \mathbb{E}_{t, \mathbf{x}_t} [\|v(\mathbf{x}_t, t) - v_\theta(\mathbf{x}_t, t)\|_2^2]. \quad (5)$$

where  $v(\mathbf{x}, t)$  can be designed in various forms. In the following, we offer a concise overview of three commonly-used variations of  $v(\mathbf{x}, t)$ : probability flow ODEs with the VP, VE, and constant velocity paths.

### 1). VP path.

$$\mathbf{x}_t \stackrel{\text{def}}{=} \alpha_t \mathbf{x}_0 + (1 - \alpha_t^2)^{\frac{1}{2}} \mathbf{x}_1, \quad (6)$$

where  $\alpha_t = e^{-\frac{1}{2} \int_0^t \beta(s) ds}$ . This Variance Preserving (VP) path aligns with the diffusion path in DDPM [19].

### 2). VE path.

$$\mathbf{x}_t \stackrel{\text{def}}{=} \mathbf{x}_0 + \alpha_t \mathbf{x}_1, \quad (7)$$

where  $\alpha_t$  is an increasing function, and  $\alpha_0 = 0$  and  $\alpha_1 \gg 1$ . This Variance Exploding (VE) path aligns with the diffusion path in SMLD [47].

### 3). Constant velocity path.

$$\mathbf{x}_t \stackrel{\text{def}}{=} (1 - t)\mathbf{x}_0 + t\mathbf{x}_1, \quad (8)$$

where  $\mathbf{x}_t$  is the linear interpolation between  $\mathbf{x}_0$  and  $\mathbf{x}_1$ . This means the velocity drives the flow following the direction  $v_t(\mathbf{x}_t, t) = \mathbf{x}_1 - \mathbf{x}_0$  for any  $t \in [0, 1]$ . We have chosen

this path due to its superior sampling efficiency and quality compared to SDE-based alternatives, as shown in recent studies [26, 29, 32].

All these designs offer a versatile and comprehensive diffusion framework that goes beyond the traditional vanilla diffusion [19, 46, 48]. Recent works have demonstrated a preference for this latent space [11], utilizing it in diverse applications such as image editing [23], inversion [39] and achieving rapid sampling in low NFE regimes [32]. These discoveries serve as inspiration for us to develop online guidance within this innovative regime, a concept we will elaborate on in the following sections.

## 4. Method

We explore self-guidance in diffusion models from two distinct perspectives. Firstly, through an offline approach, we extract guidance from diffusion models and subsequently employ it in guided diffusion training. Secondly, we directly investigate online guidance within diffusion models. Both of these perspectives will be elaborated upon in the following sections.

### 4.1. Offline guidance from pretrained diffusion model features

In this section, we assess pretrained diffusion models and utilize  $k$ -means clustering for generating embeddings that serve as guidance signals during training. To start with, let us consider the simple case of using guidance to finetune a diffusion model, of which the parameters  $\theta^*$  of the velocity network  $v_{\theta^*}$  is pretrained.

We apply a classifier-free guidance technique to the velocity network  $v_\theta$ . The model is optimized for the following loss function:

$$\mathcal{L}_{\text{offline}} = \mathbb{E}_{t, \mathbf{x}_t} \|\mathbf{x}_1 - \mathbf{x}_0 - v_\theta(\mathbf{x}_t, t, \mathbf{c})\|_2^2, \quad (9)$$

where  $\mathbf{c}$  is the conditional embedding for the guidance, to be detailed in the following paragraph. In practice  $\mathbf{c}$  is ran-

domly dropped out to be replaced by a learnable null embedding  $\emptyset$  with a pre-defined probability of  $p_{\text{drop}} = 15\%$ , so that our model preserves the ability of unconditioned generation. This configuration effectively results in  $\mathbf{v}_{\emptyset}(\mathbf{x}_t, t, \emptyset)$  approximating  $p(\mathbf{x}_1)$ , indicating that a significant portion of the network’s capacity is dedicated to conditional sampling (85%) as opposed to unconditional sampling (15%).

Our primary focus centers on investigating the feature from pretrained transformer-based network U-ViT [5] due to its clean architecture, efficiency, scalability, and strong performance, DiT [38] is also another suitable network which will explore in the future. To explore high-resolution image generation, we employ U-ViT in latent space, following the approach outlined in previous works [11, 23, 42]. We consider feature representations from various timesteps  $t$  and layer index  $l$  of the U-ViT network. In the case of offline guidance, the one-hot cluster embedding  $\mathbf{c}$  is achieved by the  $k$ -means clustering on the pretrained U-ViT features  $v_{\theta^*}(\mathbf{x}, t, \emptyset)$ . The rationale behind these choices is discussed in more detail in the ablation experiments section (see Experiment 5.2), which also motivates us to design the online guidance in the next section.

## 4.2. Bootstrap online Sinkhorn-Knopp clustering

We previously discussed offline guidance extraction from pretrained diffusion models on the U-ViT network. To enable online guidance, we integrate online clustering algorithms into the diffusion model, as shown in Figure 2.

**Sinkhorn-Knopp clustering.** Offline clustering for guidance embedding is an intuitive approach, but it suffers from issues of low efficiency and dependence on external models. Instead, we solve online clustering as an optimal transport problem using the Sinkhorn-Knopp algorithm [10] as inspired by the image-level methods in self-supervised learning [3, 7] but propose to have this *simultaneous* to the training of the diffusion model.

Our goal is to achieve guidance embeddings  $\mathbf{c}$  from the diffusion model during the training stage to boost the quality of generation by means of conditioning. The challenge arises when attempting to obtain usable signals for clustering as the conditional guidance within a diffusion model that is dependent on the conditioning.

To this end, our approach involves employing a zero vector  $\mathbf{0}$  into the conditional diffusion model  $v_{\theta}^l(\mathbf{x}_t, t, \mathbf{0})$  for the signals used to identify the clustering. Note that the zero vector  $\mathbf{0}$  needs to be discriminated from the learnable null embedding that replaces the dropped-out guidance embedding to retain of ability of high-quality unconditional generation. Particularly, for each image example,  $v_{\theta}^l(\mathbf{x}_t, t, \mathbf{0})$  undergoes a fully-connected feature prediction head  $h_{\phi}(\cdot)$ , resulting in a  $d$ -dimensional image feature embedding  $\mathbf{z} = h_{\phi}(v_{\theta}^l(\mathbf{x}_t, t, \mathbf{0})) \in \mathbb{R}^d$ , and we denote a batch of  $B$  feature

vectors as  $\mathbf{Z} = [\mathbf{z}_1, \dots, \mathbf{z}_B] \in \mathbb{R}^{B \times d}$ . To achieve online clusters, we map the column feature vectors in  $\mathbf{Z}$  to a set of  $K$  learnable prototypes  $[\mathbf{m}_1, \dots, \mathbf{m}_K] = \mathbf{M} \in \mathbb{R}^{K \times d}$  with a joint probability transportation matrix  $\mathbf{P} \in \mathbb{R}^{K \times B}$ .

In the context of the optimal transport problem,  $\mathbf{P}$  is relaxed to be an element of a transport polytope [10]:

$$\mathcal{U}(\mathbf{q}_r, \mathbf{q}_c) = \{ \mathbf{P} \in \mathbb{R}_+^{K \times B} \mid \mathbf{P}\mathbf{1} = \mathbf{q}_r, \mathbf{P}^T\mathbf{1} = \mathbf{q}_c \}, \quad (10)$$

where  $\mathbf{1}$  denotes vectors of all ones of the appropriate dimensions.  $\mathbf{q}_r \in \mathbb{R}^K$  and  $\mathbf{q}_c \in \mathbb{R}^B$  are interpreted as the marginal probability vectors of rows and columns in  $\mathbf{P}$ . Following Asano et al. [3], we adhere to the simple heuristic that  $\mathbf{P}$  evenly partitions examples into clusters to ensure diversity, *i.e.*  $\mathbf{q}_r = \mathbf{1}/B$  and  $\mathbf{q}_c = \mathbf{1}/K$ .

In the context of the optimal transport problem [10], we define the Sinkhorn-Knopp loss function as the *dual-Sinkhorn divergence* which approximates the optimal transport distance:

$$\mathcal{L}_{\text{SK}} = \langle \mathbf{P}^*, -\mathbf{M}\mathbf{Z}^T \rangle_F, \quad \text{where} \quad (11)$$

$$\mathbf{P}^* = \arg \min_{\mathbf{P} \in \mathcal{U}(\mathbf{q}_r, \mathbf{q}_c)} \langle \mathbf{P}, -\mathbf{M}\mathbf{Z}^T \rangle_F - \frac{1}{\lambda} H(\mathbf{P}). \quad (12)$$

Here  $\langle \cdot, \cdot \rangle_F$  is the Frobenius inner product.  $-\mathbf{M}\mathbf{Z}^T$  is the distance matrix between column elements in  $\mathbf{M}$  and  $\mathbf{Z}$ .  $H(\mathbf{P}^*) = -\sum_{ij} \mathbf{P}_{ij}^* \log \mathbf{P}_{ij}^*$  is the entropy term introduced by Cuturi [10] with a parameter  $\lambda > 0$ . With this term, the optimal  $\mathbf{P}^*$  can be calculated for a much cheaper cost than the original optimal transport problem in the form of:

$$\mathbf{P}^* = \text{diag}(\mathbf{r}_u) e^{-\lambda \mathbf{M}\mathbf{Z}^T} \text{diag}(\mathbf{r}_v), \quad (13)$$

where  $e^{(\cdot)}$  is the element-wise exponential, and  $\mathbf{r}_u$  and  $\mathbf{r}_v$  are renormalization vectors in  $\mathbb{R}^K$  and  $\mathbb{R}^B$ , respectively, which are calculated efficiently through a small number of matrix multiplications using the iterative Sinkhorn-Knopp algorithm [45]. We refer to [10] for derivation details.

**Joint optimizing online Sinkhorn-Knopp assignment and diffusion.** In our online bootstrapping method, we generally combine the diffusion training loss and the Sinkhorn-Knopp loss as follows:

$$\mathcal{L}_{\text{online}} = \mathcal{L}_d + \mathcal{L}_{\text{SK}}. \quad (14)$$

During the initial steps of training, challenges arise concerning feature representativeness extracted from  $v$ , resulting in a potential conflict between  $\mathcal{L}_d$  and  $\mathcal{L}_{\text{SK}}$  losses. To address this, we implement several key modifications. Firstly, we introduce a warm-up coefficient,  $\sigma$ , to control the influence of the Sinkhorn-Knopp loss,  $\mathcal{L}_{\text{SK}}$ , during the warmup stage that emphasizes more unconditional training for a good initialization of diffusion features, the second stage, we focus on training the classifier-free guidance generation,

utilizing signals from the prototype  $\mathbf{M}$ . Secondly, we use `stop-gradient` operation after extracting the features from diffusion models. Lastly, we incorporate the moving average of the U-ViT model to extract the feature.

Based on previous analysis, we design our diffusion loss  $\mathcal{L}_d$  as follows:

$$\mathcal{L}_d = \mathbb{E}_{t, \mathbf{x}_t} \|\mathbf{x}_1 - \mathbf{x}_0 - v_\theta(\mathbf{x}_t, t, \mathbf{c})\|_2^2, \quad (15)$$

where in the warmup stage, we set  $\mathbf{c} = \mathbf{0}$  as the zero vector to enable unconditional generation. In the main training stage,  $\mathbf{c}$  is extracted from the moving average of the diffusion models itself to achieve classifier-free guidance training. The condition signal  $\mathbf{c}$  is set as  $\mathbf{c} = \mathbf{m}^*$ , or with a chance of  $p_{\text{drop}} = 15\%$  to be dropped out to a learnable null embedding  $\emptyset$ , that helps to retain the ability of unconditional generation.

$$\mathbf{m}^* = \arg \max_{\mathbf{m} \in \mathbf{M}} \mathbf{m}^\top h_\phi(v_\theta^l(x_{t_s}, t_s, \mathbf{0})). \quad (16)$$

where  $\bar{\theta}$  stands for the exponential moving average of the network parameter.  $l$  and  $t_s$  are hyperparameters used to extract features from diffusion models.  $h_\phi(v_\theta^l(x_{t_s}, t_s, \mathbf{0}))$  is the image feature embedding  $\mathbf{z}$  as discussed above.

Our training process, detailed in Algorithm 1, incorporates these changes. During optimization, several parameter sets are fine-tuned, including  $\theta$  for the diffusion model,  $\phi$  for the fully connected (FC) adaptor layer,  $\mathbf{M}$  for the learnable Sinkhorn-Knopp prototypes, and  $\emptyset$  for the null embedding used in the classifier-free guidance.

**Sampling.** We use a rounding procedure [3, 7] to obtain a discrete code, which is then applied in the sampling process for bootstrapping guidance. The guidance is governed by the equation:

$$v_\theta^{\text{sample}}(\mathbf{x}_t, t, \mathbf{c}) = v_\theta(\mathbf{x}_t, t, \mathbf{c}) + g \cdot (v_\theta(\mathbf{x}_t, t, \mathbf{c}) - v_\theta(\mathbf{x}_t, t, \emptyset)), \quad (17)$$

where  $g$  represents the guidance strength that balances diversity and fidelity, and  $\mathbf{c}$  here is a prototype from  $\mathbf{M}$ .

Sampling follows the ODE in Equation 4. Utilizing estimations from Equation 5 and Equation 17, we perform backward sampling by setting  $\hat{\mathbf{x}}_0 = \int_1^0 v_\theta^{\text{sample}}(\mathbf{x}_t, t, \mathbf{c}) dt$ , given that we have access to the noise  $\mathbf{x}_1 \sim p_1$ . We solve this integration using numerical integrators.

For our guidance signal  $\mathbf{c}$ , we offer the flexibility to predefine its semantic meaning through visualization, as demonstrated in Appendix Section 11, where different prototypes embody distinct meanings. Alternatively, we can condition  $\mathbf{c}$  on a given image, leveraging a single forward pass of the network to query the most similar prototype from  $\mathbf{M}$ , and subsequently continue to condition our model on the queried prototype. This inherent flexibility is a defining feature of our framework, enhancing its adaptability and utility.

---

**Algorithm 1** Bootstrapping diffusion features for guidance by optimal transport assignment.

---

- 1: **Input:**  $\mathbf{x}_1$  the real data;  $v$  and  $\theta$  the vector field predictor with parameters;  $h$  and  $\phi$  the FC adaptor and parameters;  $\mathbf{M}$  the learnable prototypes; and  $\emptyset$  the learnable null embedding for classifier-free guidance.
  - 2: **Parameters:**  $N$  the number of iterations;  $\sigma$  the threshold for warmup, default 0.5;  $t_s$  the timestep and  $l$  the layer index for online self-guidance sampling; and  $p_{\text{drop}}$  the dropout rate.
  - 3: **for**  $iter = 1, 2, \dots, N - 1$  **do**
  - 4:   Sample  $\mathbf{x}_0 \sim \mathcal{N}(0, 1)$  from the Gaussian distribution,  $\tilde{\mathbf{x}}_0 = \mathbf{x}_0$  at  $\hat{t} = 0$ .
  - 5:   Sample  $\mathbf{x}_1$ .
  - 6:   **if**  $iter/N < \sigma$  **then**
  - 7:      $\mathcal{L}_d \leftarrow \mathbb{E}_{t, \mathbf{x}_t} \|\mathbf{x}_1 - \mathbf{x}_0 - v_\theta(\mathbf{x}_t, t, \mathbf{0})\|_2^2$
  - 8:   **else**
  - 9:     Sample  $\tilde{p} \sim \text{Bernoulli}(p_{\text{drop}})$ .
  - 10:    **if**  $\tilde{p} = 0$  **then**
  - 11:     Obtain  $\mathbf{m}^*$  from Eq. 16.
  - 12:      $\mathcal{L}_d \leftarrow \mathbb{E}_{t, \mathbf{x}_t} \|\mathbf{x}_1 - \mathbf{x}_0 - v_\theta(\mathbf{x}_t, t, \mathbf{m}^*)\|_2^2$
  - 13:    **else**
  - 14:      $\mathcal{L}_d \leftarrow \mathbb{E}_{t, \mathbf{x}_t} \|\mathbf{x}_1 - \mathbf{x}_0 - v_\theta(\mathbf{x}_t, t, \emptyset)\|_2^2$ .
  - 15:    **end if**
  - 16:   **end if**
  - 17:   Calculate  $\mathcal{L}_{\text{SK}}$  from Eq. 11.
  - 18:    $\mathcal{L} \leftarrow \mathcal{L}_d + \min(\frac{iter}{\sigma \times N}, 1.0) \times \mathcal{L}_{\text{SK}}$ .
  - 19:   Update  $\theta, \phi, \mathbf{M}, \emptyset$ .
  - 20: **end for**
  - 21: **Return:**  $\theta, \phi, \mathbf{M}, \emptyset$ .
- 

## 5. Experiments

### 5.1. Dataset, training and evaluation

**Datasets.** We report results on three datasets: ImageNet256 [12], ImageNet256-100 [14] (a subset of ImageNet-1k with 100 classes), and LSUN-Churches [57]. The ablation study is conducted on ImageNet100. We train all methods for a total of 40,000, 100,000, and 300,000 iterations on ImageNet256-100, LSUN-Churches, and ImageNet256, respectively. This training takes approximately 2 days for ImageNet256-100, 4 days for LSUN-Churches, and 12 days for ImageNet256, utilizing 4 A1000 GPUs. All methods are compared under the same hyperparameter settings (see Appendix Section 7).

**Training.** We utilize the U-ViT-Large model from U-ViT [5], which features 21 layers, 1 024 embedding dimensions, 4,096 MLP size, 16 heads, and 287M parameters. When provided with an image denoted as  $I \in \mathbb{R}^{256 \times 256 \times 3}$ , we conduct operations in the latent-space  $z \in \mathbb{R}^{32 \times 32 \times 4}$ . For sampling the prototype  $\mathbf{M}$ , we closely adhere to the distribution observed in the data. This ensures that our sampling methodology is representative and grounded in the actual data characteristics. We use  $\sigma=0.5$  during training,

and the Exponential Moving Average (EMA) is open till the Sinkhorn-Knopp loss finishes its warmup stage. When calculating the Sinkhorn-Knopp loss during the warmup stage, we mask the timestep  $t$  within the range  $[0.15, 0.25]$  to ensure that the network focuses on this specific time step for improved discriminative performance. We use the `dopri5` ODE solver for sampling, and guidance strength  $g=0.4$ . For more detailed implementation specifics we refer to the Appendix. Code will be released.

**Evaluation.** We evaluate both diversity and fidelity of the generated images by the Fréchet Inception Distance (FID) [17], as it is the most common metric for the evaluation of generative methods, e.g., [13, 22, 25, 43]. It provides a symmetric measure of the distance between two distributions in the feature space of Inception-V3 [49]. We compute the FID using 10,000 reference images and use it as our main metric for the sampling quality. We also measure the Inception Score (IS) [44], following common practice [6, 13, 22, 25]. IS measures how well a model fits into the full ImageNet class distribution.

## 5.2. Results

Our experiments comprise three main parts. Firstly, we investigate the impact of offline guidance, examining its effects concerning the timestep  $t$  and the layer index of U-ViT. Secondly, we present results from our online self-guidance experiments on ImageNet and LSUN-Churches, accompanied by several ablation studies. Lastly, we offer a range of analyses and visualizations to enhance our method’s comprehension.

**Ablation studies about offline guidance.** We conduct ablation studies on offline guidance signal extraction, considering two key factors: the timestep  $t$  and the layer index of U-ViT. Figure 3 showcases the results of our ablation study. Following [22], we employ Normalized Mutual Information (NMI) and Adjusted Rand Index (ARI) metrics to assess the effectiveness of our guidance signal in terms of clustering, with our ultimate aim being to improve fidelity. The study indicates that the optimal performance in terms of NMI and ARI is achieved at the midpoint of the model’s layers (specifically, the 10<sup>th</sup> layer in a 21-layer structure) and at the timestep of 0.2.

**Ablation studies about bootstrapping guidance.** We draw the conclusion of the optimal layer index and timestep with offline guidance, and apply this setup to our online guidance experiments, using layer index 10 and timestep 0.2. In addition, we conduct several ablation studies on the online bootstrapping learning paradigm, exploring key factors that include the necessity of `stop-gradient` to mitigate interaction between the diffusion loss and the

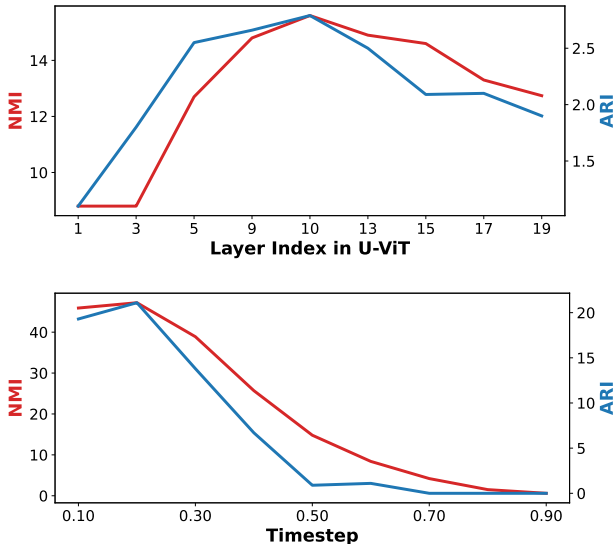


Figure 3. **Performance in clustering across various layer numbers and timesteps.** Timestep 0.2 and layer index 10 is the optimal combination.

Sinkhorn-Knopp loss, the impact of the warm-up weight (which determines reliance on a well-developed diffusion representation before applying the Sinkhorn-Knopp loss), the use of the `[CLS]` token instead of using average-pooled embeddings from patches, and the importance of masking timesteps within the range  $[0.15, 0.25]$  during bootstrapping guidance extraction to focus the network on this specific timeframe. Our findings, summarized in Table 2, emphasize the significance of these choices in optimizing FID on ImageNet256-100.

**Main results.** Incorporating our prior research findings in offline and online guidance, we present our experimental results across three distinct datasets: ImageNet256-100 (Table 1), ImageNet256, and LSUN-Churches (Table 3). We primarily compare our approach with unconditional diffusion models, class-conditioned diffusion models, and DINO guidance. For offline guidance, we employ 5,000, 300, and 30 feature clusters for ImageNet256, ImageNet256-100, and LSUN-Churches, respectively. For DINO guidance, we utilize features from DINO [8] by applying 300 clusters using  $k$ -means the one-hot embeddings are applied as the offline guidance, following a similar approach to [22]. In the case of class-conditional diffusion models, we rely on existing labels. To ensure a fair comparison, we maintain consistent training hyperparameters and model sizes across all experiments.

For ImageNet result in Table 1 and 3 (left), our proposed approaches of offline self-guidance and online self-guidance both significantly outperform unconditional diffusion models. DINO [8] slightly outperforms our online bootstrap method, suggesting potential improvements in the

	<i>anno-free</i>	<i>online</i>	FID ↓	IS ↑
Unconditional	–	–	45.1	26.5
Offline Guidance from diffusion †	✓	✗	35.8	34.8
Bootstrapping guidance	✓	✓	36.0	34.3
Bootstrapping guidance (Patch)	✓	✓	33.4	45.3
Class guidance ‡	✗	–	34.4	44.1
DINO guidance *	✓	✗	32.0	48.7

Table 1. **Main result on ImageNet256-100.** † requires pretrained diffusion model. ‡ requires GT labels as heuristics. \* requires off-the-shelf pretrained DINO encoder.

	FID ↓	IS ↑
<b>Our Method</b>	36.0	34.3
w/o stop-gradient	45.0	24.1
w/o [CLS] token	37.1	33.1
w/o warmup weight	46.1	22.1
w/o masking timestep	39.8	31.2

Table 2. **Ablation study about bootstrapping guidance on ImageNet256-100.** All four choices prove to be advantageous.



Figure 4. **The trend of Normalized Mutual Information (NMI) and FID during training.** Our generated images initially exhibit low discriminability (low NMI) and suboptimal fidelity in the first half of iterations but gradually improve in fidelity (FID) and cluster cohesiveness (high NMI) during the latter half of iterations.

	<i>ImageNet256</i>		<i>LSUN-Churches</i>	
	FID ↓	IS ↑	FID ↓	IS ↑
Unconditional	42.5	23.1	13.10	2.95
Offline guidance from diffusion †	29.8	38.1	12.75	3.03
Bootstrapping guidance	30.9	32.3	12.38	3.17
Class Guidance ‡	19.1	61.2	–	–

Table 3. **Main results on ImageNet256 and LSUN-Churches.** † with pretrained diffusion model. ‡ requires ground truth labels.

interplay between guidance signals and diffusion models for bootstrapping. However, it’s important to acknowledge that a performance gap persists when compared to class-conditioned diffusion models, which heavily depend on extensive data annotations.

We also explore the extension of patch-level bootstrapping guidance, inspired by recent advancements in self-supervised learning [9, 60]. The only major difference from our aforementioned image-level bootstrapping guidance lies in using individual patch tokens instead of the [CLS] token in U-ViT, followed by the patch-level Sinkhorn-Knopp assignment rather than on images. In Table 1, we observe that the patch-level guidance leads to better fidelity than image-level bootstrapping guidance and class guid-

ance, while the gap with DINO guidance is marginal. This more detailed guidance at the level of patches can yield better fidelity, which is in line with the observations from the literature [22, 59].

In Table 3 (right), our results on LSUN-Churches indicate that both our offline and online self-guidance approaches outperform unconditional generation, with the online self-guidance yielding the best performance.

**Training dynamics.** In Figure 4, we showcase the progression of NMI and FID during training. As training advances, both NMI and FID show consistent improvement, indicating that both feature discriminativeness and generation quality are enhanced over time, underscoring the effectiveness of our online bootstrapping method. Notably, during the warmup stage (the left half of the figure), the network predominantly focuses on unconditional generation, resulting in random images. In contrast, the model gradually adapts to generate images that align within a cluster in the later stage of training. Additional results of losses, NMI, and FID curves during training are available in Appendix Section 10.

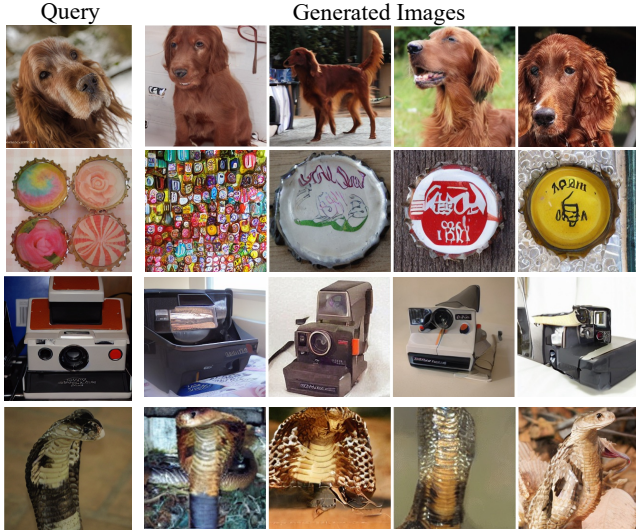


Figure 5. Using a query image in the left column for **image-level guidance**, we generate multiple images with the same prototype features. The generated images share consistent semantic meaning while exhibiting diverse appearances.

### Visualization of image-level and patch-level guidance.

Given a query image to condition our model on, we can generate multiple images that belong to the same cluster as the query, as illustrated in Figure 5. We further show the clustering of the online self-guidance in Appendix Section 10. In Figure 6, we visualize sampled images using patch-level bootstrapping guidance. It demonstrates that the generated images align well in layout with individual patches of the query images, highlighting the flexibility of our method to transition from image-level to patch-level guidance.

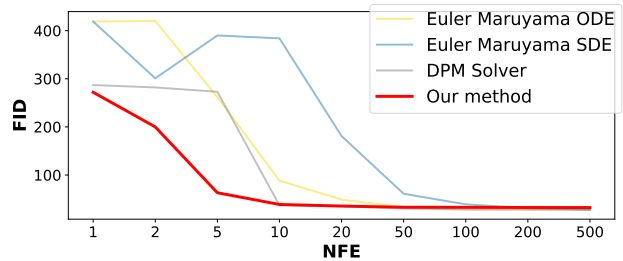
**Sampling steps.** To dissect the sampling efficiency of our method, we primarily compare with three sampling baselines: Euler-Maruyama ODE [48] and Euler-Maruyama SDE [48], and DPM solver [33]. We focus on evaluating the trade-off between Fréchet Inception Distance (FID) and the Number of Function Evaluations (NFE), as illustrated in Figure 7a. Notably, our method demonstrates a superior trade-off between sampling steps and fidelity, particularly in the low-NFE regime. Additionally, we provide visualizations of different sampling steps in Figure 7b. It is evident that sampling in just 20 steps already yields vivid results, and further increasing the number of sampling steps leads to diminishing improvements in sampling quality. This demonstrates our framework’s sampling efficiency.

## 6. Conclusion

In this paper, we introduce two frameworks for exploring self-guidance within diffusion models, allowing us to leverage their features either offline or through online self-bootstrapping. Our methods unlock the latent potential of



Figure 6. Using a query image in the left column for **patch-level guidance**, we generate multiple images with the same prototype features. The generated images maintain a consistent semantic layout while featuring diverse backgrounds and slight variations.



(a) FID v.s. NFE on ImageNet100.



(b) Visualizing clusters at different sampling steps.

Figure 7. **Results of different sampling steps.** Our method can achieve better sampling efficiency.

diffusion models during training, surpassing unconditional generation and performing comparably to class-conditioned generation. In the future, we would like to explore other similar backbone such as DiT [38] to validate the efficacy of our method.



## References

- [1] Michael S Albergo, Nicholas M Boffi, and Eric Vandenberg. Stochastic interpolants: A unifying framework for flows and diffusions. *arXiv*, 2023. 1
- [2] Brian DO Anderson. Reverse-time diffusion equation models. *Stochastic Processes and their Applications*, 12(3):313–326, 1982. 2
- [3] Yuki Markus Asano, Christian Rupprecht, and Andrea Vedaldi. Self-labelling via simultaneous clustering and representation learning. In *ICLR*, 2020. 2, 4, 5
- [4] Fan Bao, Chongxuan Li, Jiacheng Sun, and Jun Zhu. Why are conditional generative models better than unconditional ones? *arXiv*, 2022. 1, 2
- [5] Fan Bao, Chongxuan Li, Yue Cao, and Jun Zhu. All are worth words: a vit backbone for score-based diffusion models. *CVPR*, 2023. 4, 5, 12, 14
- [6] Andrew Brock, Jeff Donahue, and Karen Simonyan. Large scale gan training for high fidelity natural image synthesis. In *ICLR*, 2019. 6
- [7] Mathilde Caron, Ishan Misra, Julien Mairal, Priya Goyal, Piotr Bojanowski, and Armand Joulin. Unsupervised learning of visual features by contrasting cluster assignments. In *NeurIPS*, 2020. 2, 4, 5
- [8] Mathilde Caron, Hugo Touvron, Ishan Misra, Hervé Jégou, Julien Mairal, Piotr Bojanowski, and Armand Joulin. Emerging properties in self-supervised vision transformers. In *ICCV*, 2021. 2, 6
- [9] Mathilde Caron, Neil Houlsby, and Cordelia Schmid. Location-aware self-supervised transformers. *arXiv*, 2022. 7
- [10] Marco Cuturi. Sinkhorn distances: Lightspeed computation of optimal transport. In *NeurIPS*, 2013. 4
- [11] Quan Dao, Hao Phung, Binh Nguyen, and Anh Tran. Flow matching in latent space. *arXiv*, 2023. 3, 4
- [12] Jia Deng, Wei Dong, Richard Socher, Li-Jia Li, Kai Li, and Li Fei-Fei. ImageNet: A large-scale hierarchical image database. In *CVPR*, 2009. 1, 5
- [13] Prafulla Dhariwal and Alexander Nichol. Diffusion models beat gans on image synthesis. In *NeurIPS*, 2021. 1, 2, 6
- [14] Tian et al. Contrastive multiview coding. In *ECCV*, 2020. 5
- [15] Jia Gong, Lin Geng Foo, Zhipeng Fan, Qihong Ke, Hossein Rahmani, and Jun Liu. Diffpose: Toward more reliable 3d pose estimation. In *CVPR*, 2023. 1, 2
- [16] William Harvey and Frank Wood. Visual chain-of-thought diffusion models. *arXiv*, 2023. 1
- [17] Martin Heusel, Hubert Ramsauer, Thomas Unterthiner, Bernhard Nessler, and Sepp Hochreiter. Gans trained by a two time-scale update rule converge to a local nash equilibrium. In *NeurIPS*, 2017. 6
- [18] Jonathan Ho and Tim Salimans. Classifier-free diffusion guidance. In *NeurIPS Workshop*, 2021. 2
- [19] Jonathan Ho, Ajay Jain, and Pieter Abbeel. Denoising diffusion probabilistic models. In *NeurIPS*, 2020. 1, 2, 3, 12
- [20] Jonathan Ho, Tim Salimans, Alexey Gritsenko, William Chan, Mohammad Norouzi, and David J Fleet. Video diffusion models. In *ARXIV*, 2022. 1
- [21] Karl Holmquist and Bastian Wandt. Diffpose: Multi-hypothesis human pose estimation using diffusion models. *arXiv*, 2022. 2
- [22] Vincent Tao Hu, David W Zhang, Yuki M. Asano, Gertjan J. Burghouts, and Cees G. M. Snoek. Self-guided diffusion models. In *CVPR*, 2023. 1, 2, 6, 7
- [23] Vincent Tao Hu, David W Zhang, Pascal Mettes, Meng Tang, Deli Zhao, and Cees G.M. Snoek. Latent space editing in transformer-based flow matching. In *ICML 2023 Workshop, New Frontiers in Learning, Control, and Dynamical Systems*, 2023. 3, 4
- [24] Jindong Jiang, Fei Deng, Gautam Singh, and Sungjin Ahn. Object-centric slot diffusion. *arXiv*, 2023. 2
- [25] Tero Karras, Samuli Laine, and Timo Aila. A style-based generator architecture for generative adversarial networks. In *CVPR*, 2019. 6
- [26] Tero Karras, Miika Aittala, Timo Aila, and Samuli Laine. Elucidating the design space of diffusion-based generative models. In *NeurIPS*, 2022. 1, 2, 3, 12
- [27] Sangyun Lee, Beomsu Kim, and Jong Chul Ye. Minimizing trajectory curvature of ode-based generative models. *ICML*, 2023. 2, 12
- [28] Ziyi Li, Qinye Zhou, Xiaoyun Zhang, Ya Zhang, Yanfeng Wang, and Weidi Xie. Open-vocabulary object segmentation with diffusion models. In *ICCV*, 2023. 2
- [29] Yaron Lipman, Ricky TQ Chen, Heli Ben-Hamu, Maximilian Nickel, and Matt Le. Flow matching for generative modeling. *ICLR*, 2023. 1, 3, 12, 13
- [30] Jie Liu, Tao HU, Jan Jakob Sonke, and Efstratios Gavves. Beyond generation: Exploring generalization of diffusion models in few-shot segmentation. In *NeurIPS Diffusion Workshop*, 2023. 2
- [31] Xingchao Liu, Chengyue Gong, and Qiang Liu. Flow straight and fast: Learning to generate and transfer data with rectified flow. *arXiv*, 2022. 1
- [32] Xingchao Liu, Chengyue Gong, and Qiang Liu. Flow straight and fast: Learning to generate and transfer data with rectified flow. *ICLR*, 2023. 3, 13
- [33] Cheng Lu, Yuhao Zhou, Fan Bao, Jianfei Chen, Chongxuan Li, and Jun Zhu. Dpm-solver: A fast ode solver for diffusion probabilistic model sampling in around 10 steps. 2022. 8
- [34] Chong Mou, Xintao Wang, Jiechong Song, Ying Shan, and Jian Zhang. Dragondiffusion: Enabling drag-style manipulation on diffusion models. 2023. 1, 2
- [35] Soumik Mukhopadhyay, Matthew Gwilliam, Vatsal Agarwal, Namitha Padmanabhan, Archana Swaminathan, Srinidhi Hegde, Tianyi Zhou, and Abhinav Shrivastava. Diffusion models beat gans on image classification. 2023. 2
- [36] Anton Obukhov, Maximilian Seitzer, Po-Wei Wu, Semen Zhydenko, Jonathan Kyl, and Elvis Yu-Jing Lin. High-fidelity performance metrics for generative models in pytorch, 2020. 12
- [37] Gaurav Parmar, Richard Zhang, and Jun-Yan Zhu. On aliased resizing and surprising subtleties in gan evaluation. In *CVPR*, 2022. 12
- [38] William Peebles and Saining Xie. Scalable diffusion models with transformers. *arXiv*, 2022. 4, 8

- [39] Ashwini Pople, Matthew J Muckley, Ricky TQ Chen, and Brian Karrer. Training-free linear image inversion via flows. *arXiv*, 2023. 3
- [40] Zhongwei Qiu, Qiansheng Yang, Jian Wang, Xiyu Wang, Chang Xu, Dongmei Fu, Kun Yao, Junyu Han, Errui Ding, and Jingdong Wang. Learning structure-guided diffusion model for 2d human pose estimation. *arXiv*, 2023. 2
- [41] Alec Radford, Jong Wook Kim, Chris Hallacy, Aditya Ramesh, Gabriel Goh, Sandhini Agarwal, Girish Sastry, Amanda Askell, Pamela Mishkin, Jack Clark, et al. Learning transferable visual models from natural language supervision. In *ICML*, 2021. 1
- [42] Robin Rombach, Andreas Blattmann, Dominik Lorenz, Patrick Esser, and Björn Ommer. High-resolution image synthesis with latent diffusion models. In *CVPR*, 2022. 1, 2, 4
- [43] Chitwan Saharia, William Chan, Saurabh Saxena, Lala Li, Jay Whang, Emily Denton, Seyed Kamyar Seyed Ghasemipour, Burcu Karagol Ayan, S Sara Mahdavi, Rapha Gontijo Lopes, et al. Photorealistic text-to-image diffusion models with deep language understanding. In *ARXIV*, 2022. 1, 2, 6
- [44] Tim Salimans, Ian Goodfellow, Wojciech Zaremba, Vicki Cheung, Alec Radford, and Xi Chen. Improved techniques for training gans. In *NeurIPS*, 2016. 6
- [45] Richard Sinkhorn and Paul Knopp. Concerning nonnegative matrices and doubly stochastic matrices. *Pacific Journal of Mathematics*, 21(2):343–348, 1967. 4
- [46] Jascha Sohl-Dickstein, Eric Weiss, Niru Maheswaranathan, and Surya Ganguli. Deep unsupervised learning using nonequilibrium thermodynamics. In *ICML*, 2015. 2, 3
- [47] Yang Song and Stefano Ermon. Generative modeling by estimating gradients of the data distribution. *arXiv*, 2019. 1, 2, 3, 12
- [48] Yang Song, Jascha Sohl-Dickstein, Diederik P Kingma, Abhishek Kumar, Stefano Ermon, and Ben Poole. Score-based generative modeling through stochastic differential equations. In *ICLR*, 2021. 2, 3, 8, 12, 13
- [49] Christian Szegedy, Vincent Vanhoucke, Sergey Ioffe, Jon Shlens, and Zbigniew Wojna. Rethinking the inception architecture for computer vision. In *CVPR*, 2016. 6
- [50] Luming Tang, Menglin Jia, Qianqian Wang, Cheng Perng Phoo, and Bharath Hariharan. Emergent correspondence from image diffusion. *arXiv*, 2023. 1, 2
- [51] Haiping Wang, Yuan Liu, Bing Wang, Yujing Sun, Zhen Dong, Wenping Wang, and Bisheng Yang. Freereg: Image-to-point cloud registration leveraging pretrained diffusion models and monocular depth estimators. *arXiv*, 2023. 2
- [52] Lemeng Wu, Dilin Wang, Chengyue Gong, Xingchao Liu, Yunyang Xiong, Rakesh Ranjan, Raghuraman Krishnamoorthi, Vikas Chandra, and Qiang Liu. Fast point cloud generation with straight flows. In *CVPR*, 2023. 1
- [53] Ziyi Wu, Jingyu Hu, Wuyue Lu, Igor Gilitschenski, and Animesh Garg. Slotdiffusion: Object-centric generative modeling with diffusion models. *arXiv preprint arXiv:2305.11281*, 2023. 2
- [54] Jiarui Xu, Sifei Liu, Arash Vahdat, Wonmin Byeon, Xiaolong Wang, and Shalini De Mello. Open-vocabulary panoptic segmentation with text-to-image diffusion models. In *CVPR*, 2023. 2
- [55] Xingyi Yang and Xinchao Wang. Diffusion model as representation learner. In *ICCV*, 2023. 1, 2
- [56] Zebin You, Yong Zhong, Fan Bao, Jiacheng Sun, Chongxuan Li, and Jun Zhu. Diffusion models and semi-supervised learners benefit mutually with few labels. *NeurIPS*, 2023. 2
- [57] Fisher Yu, Yinda Zhang, Shuran Song, Ari Seff, and Jianxiong Xiao. Lsun: Construction of a large-scale image dataset using deep learning with humans in the loop. In *ARXIV*, 2015. 5
- [58] Guanqi Zhan, Chuanxia Zheng, Weidi Xie, and Andrew Zisserman. What does stable diffusion know about the 3d scene? *arXiv*, 2023. 2
- [59] Y Zhou, R Zhang, C Chen, C Li, C Tensmeyer, T Yu, J Gu, J Xu, and T Sun. Lafite: Towards language-free training for text-to-image generation. *arXiv* 2021. *arXiv*. 7
- [60] Adrian Ziegler and Yuki M Asano. Self-supervised learning of object parts for semantic segmentation. In *CVPR*, 2022. 7

# **Guided Diffusion from Self-Supervised Diffusion Features**

Supplementary Material

## Contents

<b>1. Introduction</b>	<b>1</b>
<b>2. Related works</b>	<b>2</b>
<b>3. Preliminaries</b>	<b>2</b>
<b>4. Method</b>	<b>3</b>
4.1. Offline guidance from pretrained diffusion model features . . . . .	3
4.2. Bootstrap online Sinkhorn-Knopp clustering . . . . .	4
<b>5. Experiments</b>	<b>5</b>
5.1. Dataset, training and evaluation . . . . .	5
5.2. Results . . . . .	6
<b>6. Conclusion</b>	<b>8</b>
<b>7. Hyperparameters</b>	<b>12</b>
<b>8. Extra Related Works</b>	<b>12</b>
<b>9. Method Details</b>	<b>13</b>
<b>10 Experimental Results</b>	<b>16</b>
<b>11 Visualization Results</b>	<b>16</b>

## 7. Hyperparameters

**Training Hyperparameters** In practice, we observe that using only 3 iterations in Sinkhorn-Knopp Algorithm is fast and sufficient to obtain good performance.

In offline guidance, as the pretrained weight from U-ViT is trained with classifier-free guidance, we set the conditional embedding to null to facilitate feature extraction.

Please refer to Table 4 for additional training hyperparameters, and to Table 5 for details about the training device and time.

**Network structures** We primarily investigate the network structure from U-ViT [5]. For completeness, we have replicated it in Figure 8.

**Evaluation details** We use the common package Clean-FID [37], torch-fidelity [36] for FID, IS calculation, respectively. For the checkpoint, we pick the checking point every 4,000 iterations by minimal FID between generated sample set and the train set. We utilize the precomputed mean and standard deviation statistics from U-ViT [5].

**Other attempts** We also considered adding a queue of size 5,120, which is 10 times the batch size of 512. However, we have empirically found that it does not provide any additional benefits.

## 8. Extra Related Works

**SDE and ODE in Diffusion models.** Score-based generative model family features seminal models like Score Matching with Langevin Dynamics (SMLD) by Song et al. [47], and DDPMs by Ho et al. [19]. Both SMLD and DDPMs are encompassed within the Stochastic Differential Equations (SDEs) framework, a concept further elaborated by Song et al. [48]. Recent advancements, as illustrated by Karras et al. [26] and Lee et al. [27], have shown that utilizing an Ordinary Differential Equation (ODE) sampler for diffusion SDEs can significantly reduce sampling costs compared to traditional methods involving the discretization of diffusion SDEs. Additionally, within the context of Flow Matching regimes [29] and Rectified

Dataset	ImageNet100×256	ImageNet×256	LSUN-Churches×256
Latent space	✓	✓	✓
Latent shape	32×32×4	32×32×4	32×32×4
Image decoder	ft-EMA	ft-EMA	ft-EMA
Batch size	512	512	512
Training iterations	40K	300K	100k
Warm-up steps	5K	5K	5K
Cluster Number	300	5,000	30
Optimizer	AdamW	AdamW	AdamW
Learning rate	5e-5	5e-5	5e-5
Weight decay	0.00	0.00	0.00
Betas	(0.9, 0.999)	(0.9, 0.999)	(0.9, 0.999)
Noise schedule	OT	OT	OT
Sampler	dopri	dopri	dopri
CFG	✓	✓	✓
$p_{\text{uncond}}$	0.1	0.1	0.1
Guidance strength	0.4	0.4	0.4
Convolution	×	×	×

Table 4. The experimental setup for U-ViT in the main paper. “ft-EMA” and “original” correspond to different weights of the image decoder provided in <https://huggingface.co/stabilityai/sd-vae-ft-ema>. “OT” denotes the OT path in flow matching [29, 32]. “ $p_{\text{uncond}}$ ” represents the unconditional training probability in classifier free guidance (CFG). “Convolution” represents whether to add a 3×3 convolutional block before output.

Dataset	Model	Training devices	Training time	Training iterations
ImageNet100×256	U-ViT-L/2	4 GeForce RTX A5000	48 hours	40K
LSUN-Churches×256	U-ViT-L/2	4 GeForce RTX A5000	96 hours	100K
ImageNet×256	U-ViT-L/2	4 GeForce RTX A5000	290 hours	300K

Table 5. The training devices and time.

Flow [32], both SMLD and DDPMs can be considered as special cases under the Variance Preserving and Variance-Explosion paths of the Probability Flow ODE framework [48]. We focus on the ODE approach as opposed to the traditional SDE method, a pivot that promises new insights and efficiencies in the development of generative models.

Several [29, 32] pointed out that using a non-linear interpolation for  $\mathbf{x}_t$  in the VP probability flow ODE in Equation 6 can result in an unnecessary increase in the curvature of generative trajectories. As a consequence, this can lead to reduced efficiency in the training and sampling of generative trajectories.

## 9. Method Details

**Semantic Assignment for self-learned clusters.** Sampling can be conducted under specific guidance signals. These samples can then be visualized and semantically interpreted, as demonstrated in Figure 9 (ImageNet256) and Figure 10 (LSUN-Churches).

**ODE Sampling.** We illustrate the pseudo-code for ODE sampling in Algorithm 2.

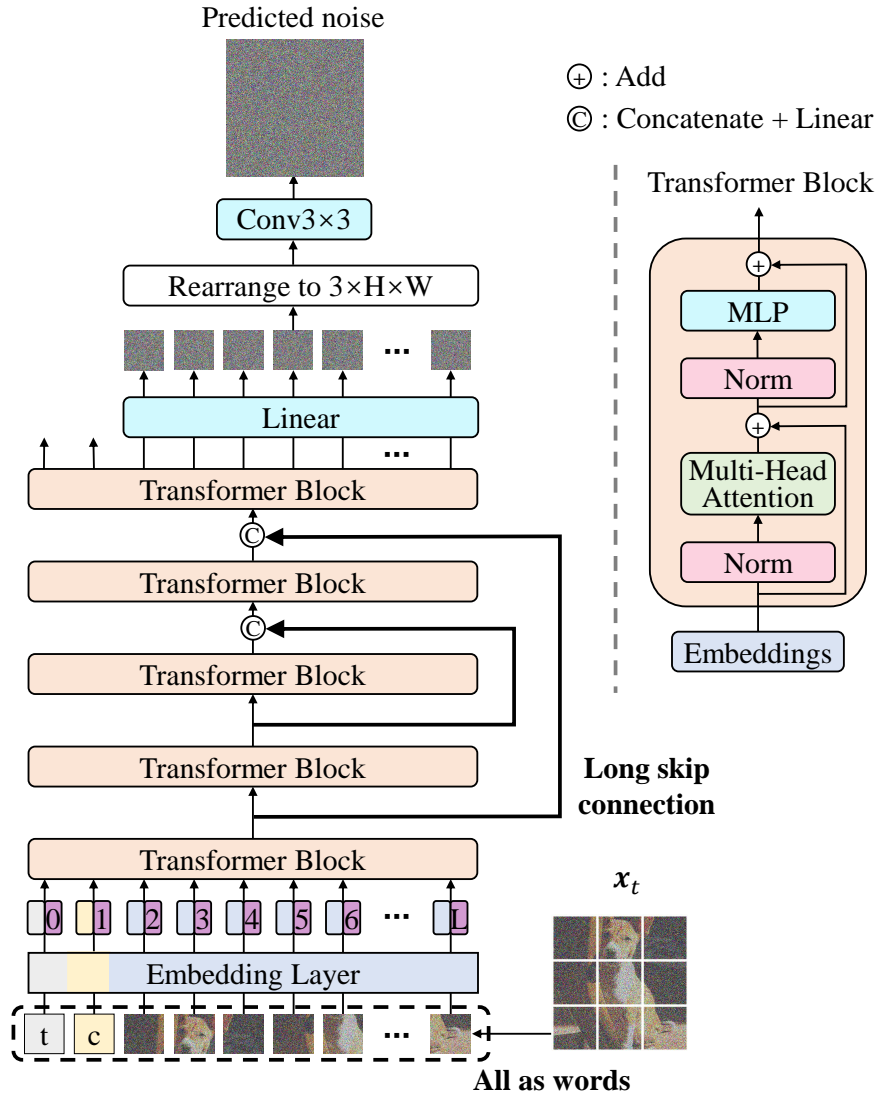


Figure 8. The U-ViT architecture for diffusion models, which is characterized by treating **all** inputs including the time, condition and noisy image patches **as tokens** and employing  $(\#Blocks-1)/2$  **long skip connections** between shallow and deep layers. The network structure is not our contribution. For completeness, this figure is replicated from the paper [5].

---

**Algorithm 2** Euler Sampling algorithm.

---

```

def ode_sampling(model, noise, x0):
    # x0: gaussian noise.
    # model: pretrained vector field predictor
    z = noise.detach().clone()
    dt = 1.0 / N
    est, traj = [], []

    for i in range(0, N, 1): # fix-step Euler ODE solver
        t = i / N
        pred = model(z, t) # vector field prediction
        pred = pred.detach().clone()
        _est_now = z + (1 - t)*pred
        est.append(_est_now)

        z = z.detach().clone() + pred * dt
        traj.append(z.detach().clone())

    return traj[-1], est

```

---



(a) Cluster #3: “dogs with dark color.”



(b) Cluster #8: “A scene with branchy trees alongside a road.”



(c) Cluster #10: “A retail store displays a wide range of goods, from everyday necessities to treats and leisure items.”

Figure 9. Semantic Interpretation: the visualization of ImageNet256 from various clusters.

**The training process of diffusion framework.** For the sake of completeness, we reiterate the algorithm of training outlined in Algorithm 3.

---

**Algorithm 3** The training process of diffusion framework.

---

- 1: **Input:** Empirical distribution  $q_1$ , gaussian distribution  $q_0$ , batchsize  $b$ , initial network  $v_\theta$ .
  - 2: **while** Training **do**
  - 3:   Sample batches of size  $b$  *i.i.d.* from the datasets
  - 4:    $\mathbf{x}_0 \sim q_0(\mathbf{x}_0)$ ;    $\mathbf{x}_1 \sim q_1(\mathbf{x}_1)$
  - 5:    $t \sim \mathcal{U}(0, 1)$
  - 6:   # Interpolation.
  - 7:    $x_t \leftarrow tx_1 + (1 - t)x_0$
  - 8:    $\text{DM}(\theta) \leftarrow \|v_\theta(x_t, t) - (\mathbf{x}_1 - \mathbf{x}_0)\|^2$
  - 9:    $\theta \leftarrow \text{Update}(\theta, \nabla_\theta \text{DM}(\theta))$
  - 10: **end while**
  - 11: **Return** DM
-



(a) Cluster #1: “cathedrals or large churches photographed at various times during the evening or night.”



(b) Cluster #4: “Each image features church buildings, depicted using different artistic styles or filter effects. These effects provide a varied aesthetic to the images, suggesting an exploration of the churches through diverse visual interpretations, likely for artistic or illustrative purposes.”



(c) Cluster #7: “All feature prominent church buildings, which showcase a variety of architectural styles from different historical periods and cultural contexts.”

Figure 10. Semantic Interpretation: the visualization of churches from various clusters out of 30.

## 10. Experimental Results

**Guidance strength v.s. FID.** Figure 11 illustrates the relationship between FID and guidance strength, revealing an optimal point for achieving the highest fidelity in FID.

**Loss curve and NMI.** In Figure 12, we display the loss and NMI trends during training. Our loss shows stable convergence, and NMI steadily rises throughout training. This indicates the increasing discriminative power of the evolving features.

## 11. Visualization Results

**Visualization of various guidance strength.** We visually showcase samples across different guidance strengths in Figure 14 and 13. These illustrations illustrate that as the guidance strength ( $g$ ) increases, the generated images exhibit higher levels of realism.



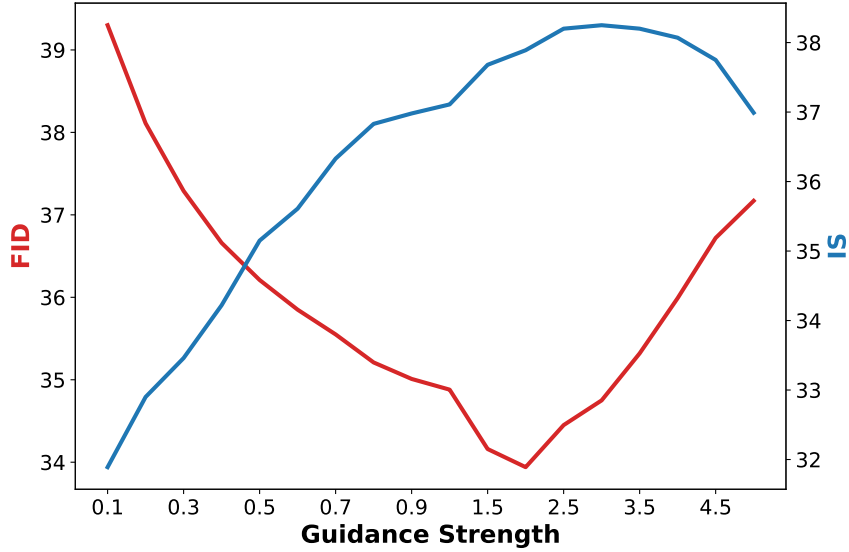


Figure 11. The influence of guidance strength for offline guidance on ImageNet100 dataset.

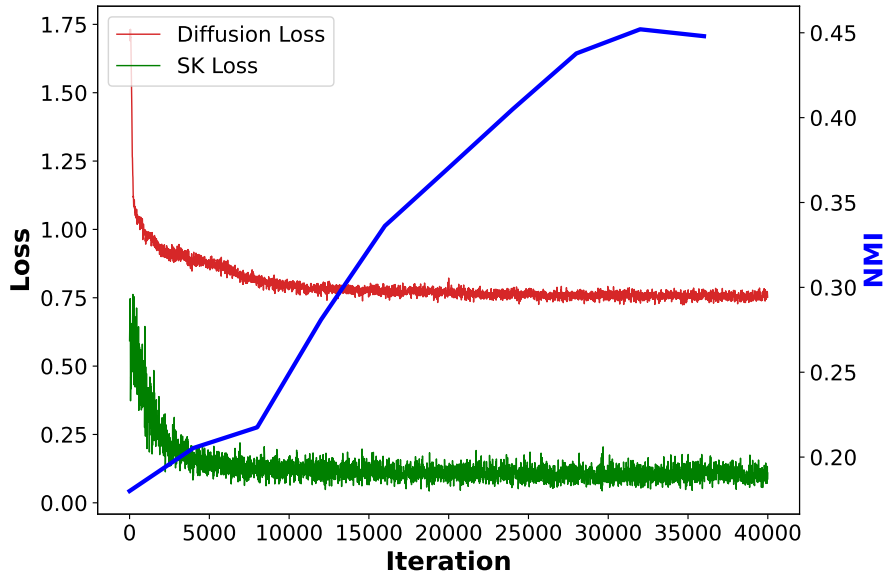


Figure 12. The trend of Normalized Mutual Information (NMI) with respect to different loss functions during training.

**FID trend.** In Figure 15, we compare the FID trends with unconditional and class-conditioned diffusion models. Initially, our method converges at a rate similar to that of unconditional diffusion models, but in the later stages, it converges more rapidly, achieving comparable levels to class-conditional diffusion models.

**Clustering non-collapse Assignment.** To further analyze the clustering of our learned prototypes, we summarize the histogram of cluster assignments in Figure 16, providing evidence of non-collapse assignment during our training.

**Cluster Visualization.** We provide visualizations of the offline clustering results in Figure 17, showcasing the discriminative nature of features from diffusion models and the similarity in color and species of the generated images.

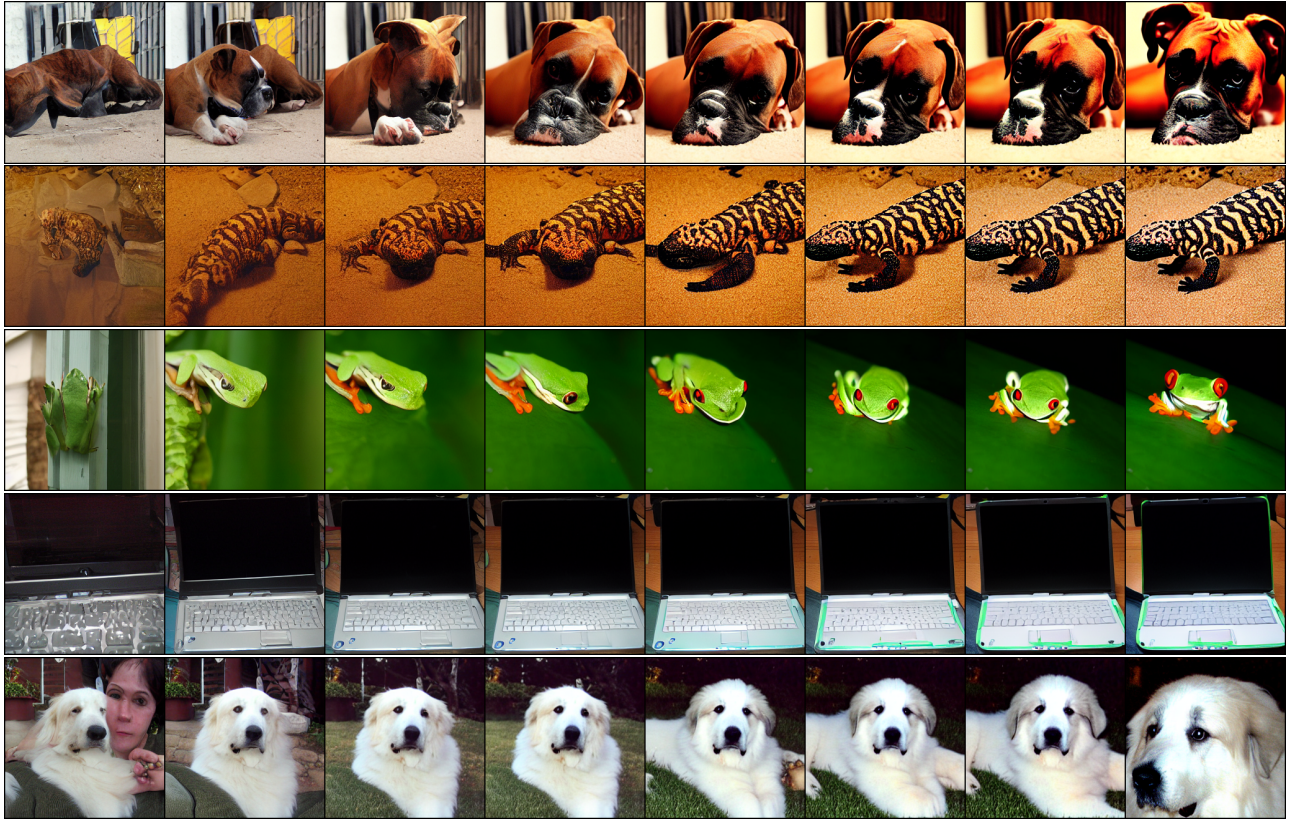


Figure 13. The visualization of incrementally increasing the guidance strength from 0 to 0.4 in flow matching on self-guidance within ImageNet256.



Figure 14. The visualization of incrementally increasing the guidance strength from 0 to 0.5 in flow matching on self-guidance within Churches256.

**Diffusion Chains Visualization.** We illustrate the estimation of  $x_1$  during sampling in Figure 19 (for ImageNet256) and in Figure 20 (for LSUN-Churches256).

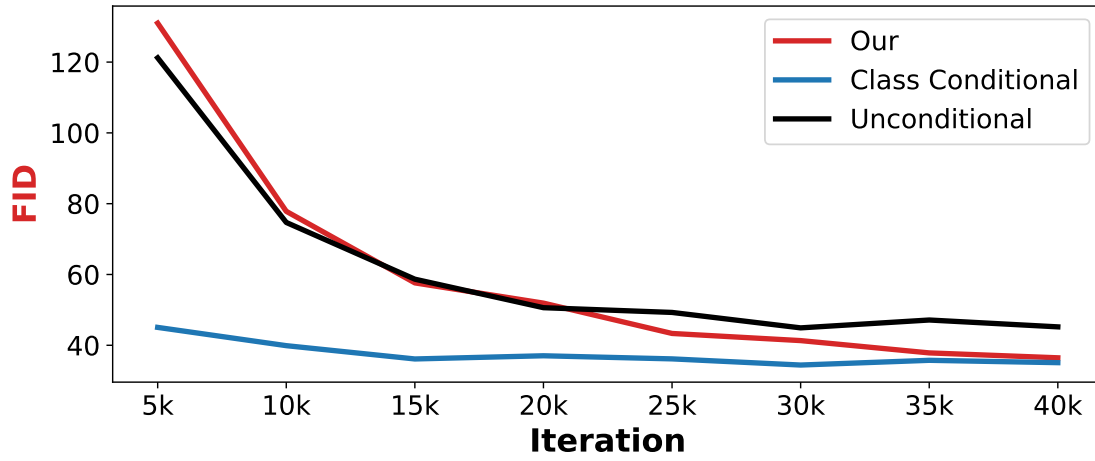


Figure 15. Trend in FID compared to unconditional diffusion models.

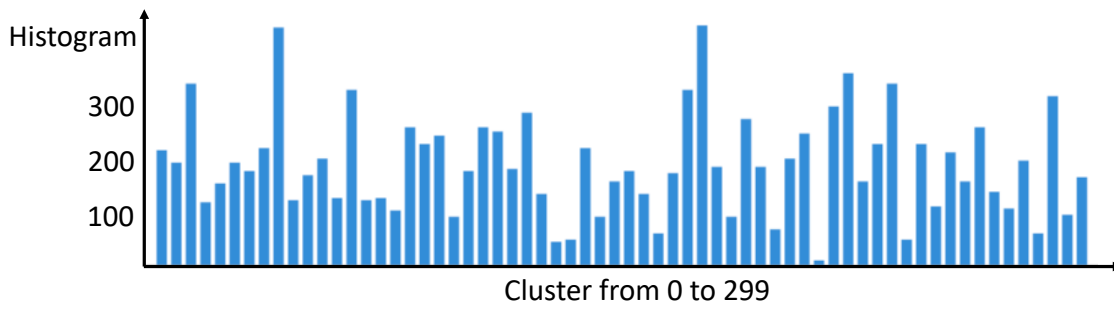


Figure 16. Histogram of cluster assignments in ImageNet100 with 300 clusters.

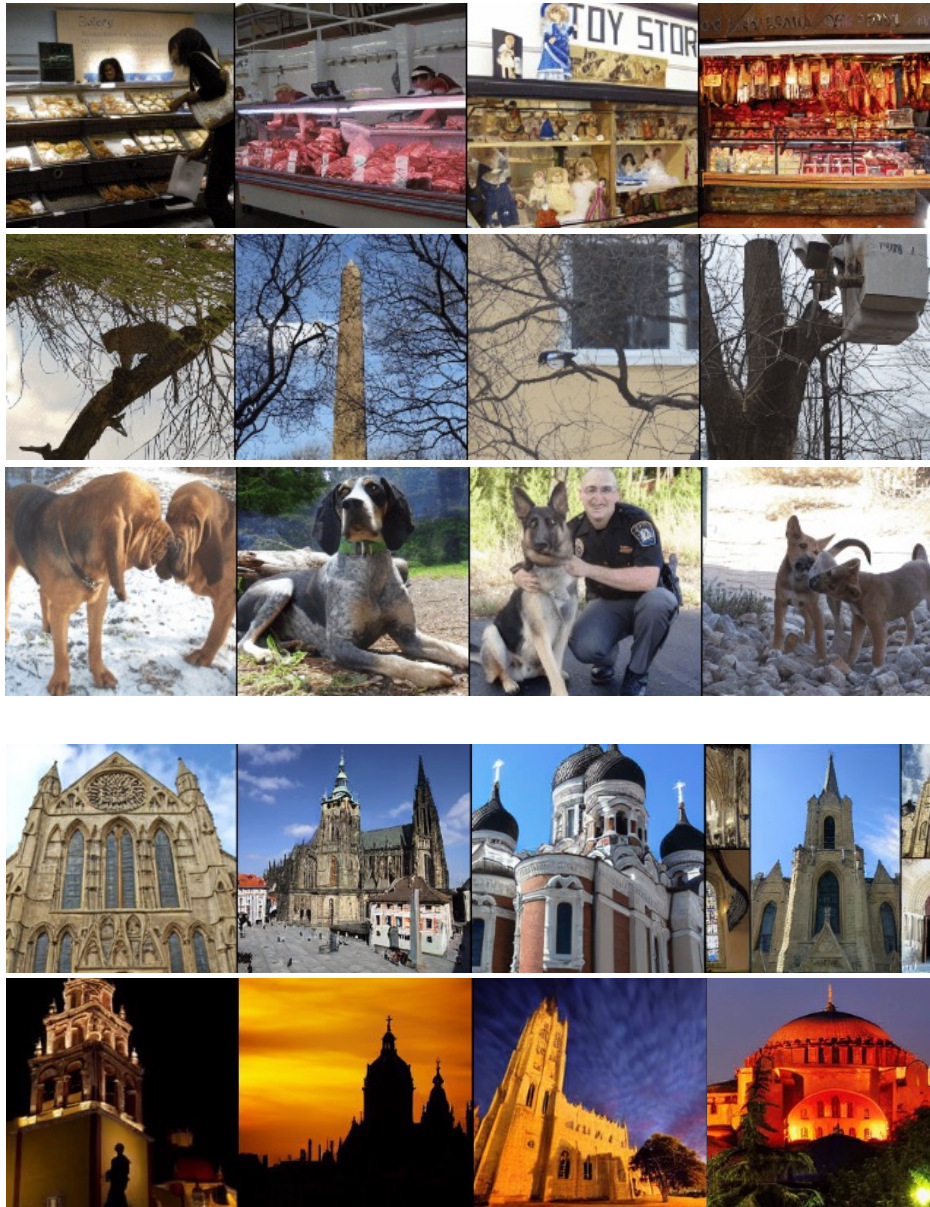


Figure 17. Cluster visualization of ImageNet256 and Churches.

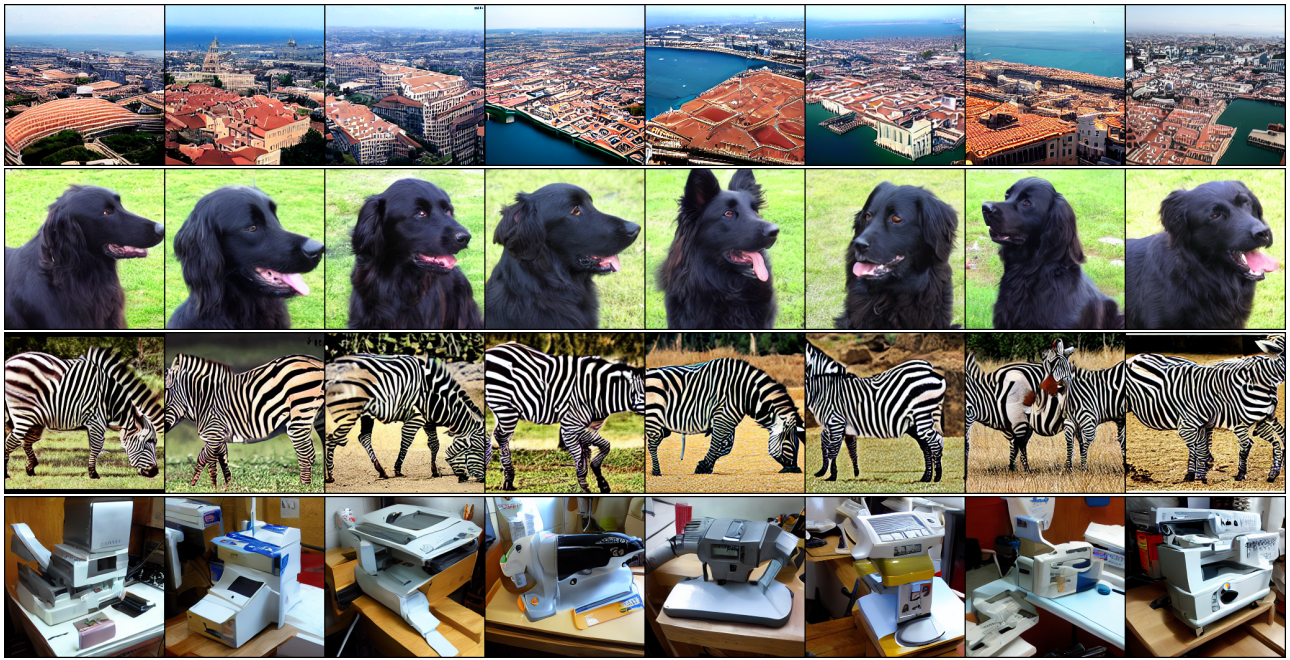


Figure 18. Offline guidance sampling visualization from different cluster ids.

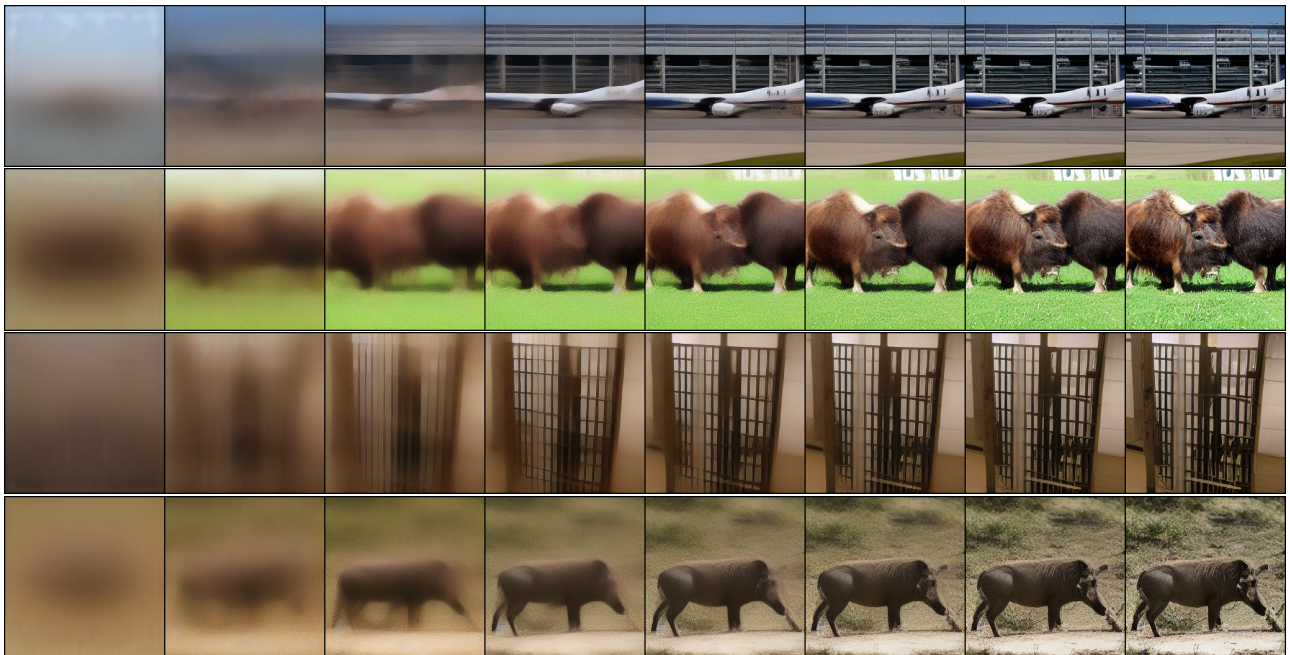


Figure 19. The visualization of the estimation of  $x_1$  on ImageNet256 during sampling with a guidance strength set to 0.4.



Figure 20. The visualization of the estimation of  $x_1$  on Churches256 during sampling with a guidance strength set to 0.4.